Nuclear Materials and Energy 26 (2021) 100939

Contents lists available at ScienceDirect

Nuclear Materials and Energy

journal homepage: www.elsevier.com/locate/nme

Quantifying erosion and retention of silicon carbide due to D plasma irradiation in a high-flux linear plasma device

G. Sinclair [a,b,*], T. Abrams [b], S. Bringuier [b], D.M. Thomas [b], L. Holland [b], S. Gonderman [b], J. H. Yu [b,c], R.P. Doerner [c]

[a] Oak Ridge Associated Universities, Oak Ridge, TN 37830, USA
[b] General Atomics, San Diego, CA 92186, USA
[c] University of California, San Diego, La Jolla, CA 92093, USA

ARTICLE INFO

Keywords:
Silicon carbide
Plasma facing materials
Fuel retention
Chemical erosion
Optical emission spectroscopy

ABSTRACT

Silicon carbide (SiC) may be a viable option for future plasma-facing components (PFCs) due to its low hydrogenic diffusivity, high temperature strength, and mechanical resilience to neutron damage (Causey et al., 1978). The erosion and retention properties of SiC were quantified via deuterium plasma exposures in the PISCES-E RF plasma source on SiC-coated graphite samples at impact energies between 20 eV and 90 eV, surface temperatures of 500 K and 950 K, and fluences between 0.4 and 1.0 $\times$ 10^{24} m^{-2}. The chemical sputtering yield of carbon from SiC was estimated by optical spectroscopy, varying between 0.0012 and 0.0083 depending on the deuterium impact energy. Chemical sputtering yields from graphite were 4$\times$ higher, on average, than yields from SiC and were largely consistent with previous analytic formulations. Chemical erosion of silicon atoms from SiC was not detected from the SiD molecular band, but the lack of Si surface enrichment at low E_i suggests that a non-collisional Si erosion source may be present. The retention of implanted deuterium in SiC was ~2$\times$ higher than that in tungsten at 500 K. Most D retained in SiC was desorbed at a peak temperature ~1000 K, and the desorption rate only varied slightly with impact energy and surface temperature. Fundamental differences in desorption behavior between Si, graphite, and SiC samples suggested that the SiC cubic lattice possessed unique trapping sites that cannot solely be attributed to Si-D or C-D bonds. New questions regarding preferential erosion and uncharacterized defects motivate expanded testing in linear and toroidal devices.

1. Introduction

Next-step fusion devices will require the use of high-performance plasma facing components (PFCs) that can survive in a nuclear radiation environment. Silicon carbide (SiC) may be a promising low-to-medium-Z material candidate for future PFCs due to its low hydrogenic diffusivity and excellent mechanical and thermal properties under neutron irradiation [2–4]. The ARIES-AT blanket concept proposed using SiC as a plasma-facing material (PFM) [5]. While extensive research has been conducted on the viability of SiC for use as a structural material [6–10], plasma material interaction studies on SiC remain sparse, particularly at high plasma fluxes [11–16].

Maintaining low PFC erosion is critical to ensuring long component lifetimes and minimizing plasma contamination. Fuel dilution and radiative losses place strict limits on acceptable levels of erosion for different PFC candidate materials [17]. The overall gross erosion of SiC may be up to 10$\times$ lower than that of graphite during deuterium (D) plasma bombardment in reactor-relevant conditions [13]. SiC mass loss has been observed during D^+ ion bombardment at impact energies below the physical sputtering threshold (~30 eV), indicating the occurrence of erosion via chemical processes, as is commonly observed in graphite [11,14,18]. A follow-up study performed in [12] verified the presence of chemical erosion via the detection of methane (CD_4) emission using *in situ* mass spectroscopy. Silane (SiD_4) emission was not measured in that experiment, despite the lack of change in the measured Si:C surface composition ratio, suggesting that Si was eroded via some process other than physical sputtering. A separate study performed at similar plasma impact energies and fluxes did measure Si surface enrichment after plasma exposure [14]. The ambiguity regarding the presence and intensity of Si-based chemical erosion motivates further work to qualify SiC as a viable PFM.

The hydrogenic retention properties in SiC must also be quantified,

* Corresponding author at: General Atomics, San Diego, CA 92186, USA.
E-mail address: sinclairg@fusion.gat.com (G. Sinclair).

https://doi.org/10.1016/j.nme.2021.100939
Received 8 December 2020; Received in revised form 26 January 2021; Accepted 1 February 2021
Available online 8 February 2021

since radioactive tritium (T) may become trapped at defects in the lattice via energetic implantation and at the surface via co-deposition with redeposited impurity ions [19]. For the purposes of this manuscript, "retention" will hereafter refer to retention due to implantation unless otherwise stated. A few studies have characterized the fundamental retention properties of SiC when exposed to fusion-relevant D^+ ion bombardment. Two major SiC desorption peaks have been observed around 800–900 K and 1000–1100 K [20,21]. Si and C samples were exposed to similar 1 keV D_2^+ ion irradiations; major desorption peaks were observed around 800 K and 1000 K, respectively [21]. Authors concluded that the low-temperature desorption peak may correspond to trapping of D atoms by Si atoms and the high-temperature desorption peak may correspond to trapping of D atoms by C atoms in the SiC lattice [21]. However, the effect of D^+ ion impact energy (sub-keV) on trapping energies and overall retention has not yet been studied; energy-dependent implantation depth and dislocation density may significantly affect long-term T inventory. In addition, measurements made in [22] indicate that SiC has very low hydrogenic diffusivity. Work in [2] demonstrated that a near-surface (~1 μm) SiC interlayer may effectively inhibit diffusion of incident D^+ ions into bulk tungsten. Both computational and experimental estimates of hydrogenic permeability were lower in SiC than in graphite and many refractory metals (e.g. W, Mo, Nb, V) over a range of surface temperatures [1,23]. Despite these promising diffusivity and permeability characteristics, no systematic study has been performed until now to quantify differences in hydrogenic retention between SiC and other PFM candidates.

The study below builds upon previous work by further defining the erosion and retention properties of SiC during fusion-relevant plasma bombardment. As mentioned previously, current knowledge on the viability of SiC as a PFM remains limited, but findings of low erosion (compared to graphite) and low hydrogenic diffusivity published over the last two decades indicate significant promise and warrant further investigation. D plasma exposures were conducted on SiC samples fabricated in-house at General Atomics at different sample temperatures and ion impact energies using the PISCES linear plasma devices at the University of California, San Diego (UCSD) [24,25]. Physical/chemical erosion and deuterium retention were examined via *in situ* and post-mortem characterization techniques. Simultaneous exposures with multiple samples were conducted to provide direct performance comparisons between select PFM candidate materials. This study complements concurrent modeling and experiments conducted in the DIII-D tokamak using the Divertor Materials Evaluation System (DiMES) [26,27] to qualify the performance of SiC-based PFCs.

2. Experimental setup

Plasma exposures were conducted using the PISCES-E plasma simulator (Fig. 1(a)) and the PISCES-A reflex arc plasma source at UCSD [24,25,28]. SiC samples were fabricated at General Atomics via chemical vapor deposition (CVD) on a graphite substrate. Each graphite sample was cut from a GrafTech ATJ^{TM} graphite rod into a "top-hat" shape shown in Fig. 1(c), with a circular plasma-facing surface measuring 6 mm in diameter. Samples were then coated with ~100–150 μm of SiC via CVD in a device described in [29]. The cubic, β-SiC coated samples were then ultrasonically cleaned using acetone and ethanol and then outgassed to ~1310 K (0.5 K s^{-1} ramp) for 1 hr to achieve a reference state for deuterium retention measurements. Some experiments were conducted with a single SiC sample, while others were conducted with four samples (CVD SiC, ATJ^{TM} graphite (2% porosity), polycrystalline tungsten (W, 99.95% purity from Midwest Tungsten Service, Inc.), and ⟨100⟩ silicon (Si, 99.99% purity from Insaco Inc.)) simultaneously to provide direct comparisons on material response (see Fig. 1(b) for images of the two sample holder geometries used in the experiment). All additional samples used in the experiment were of the same dimension as the SiC sample and underwent the same cleaning and outgassing process described above.

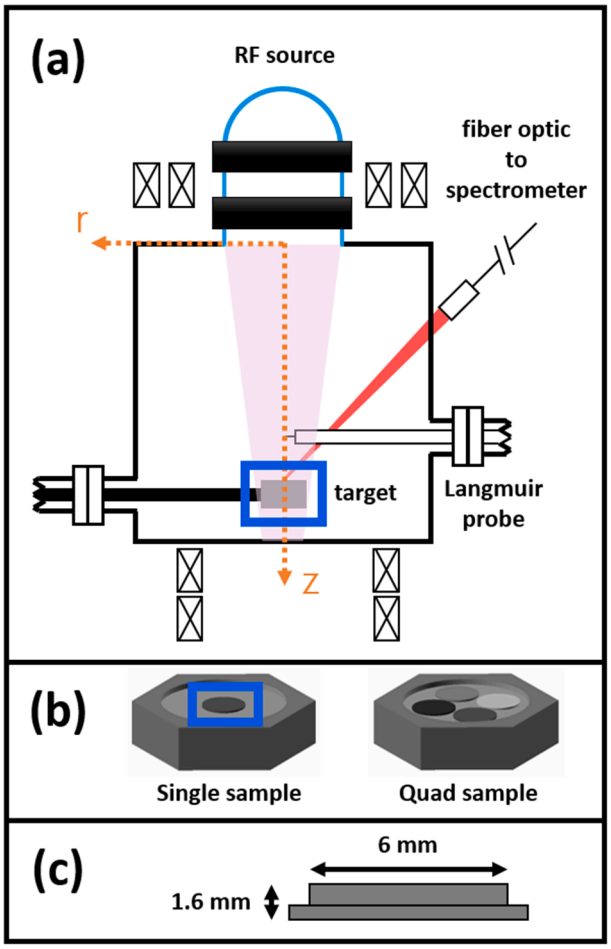

Fig. 1. (a) PISCES-E experimental setup schematic, with (b) inset showing both sample holder geometries used in plasma exposures, with (c) inset showing side view of sample geometry and dimension.

Deuterium plasma exposures performed in PISCES-E utilized 1.4–1.5 kW RF power, with an electron density (n_e) ~3 × 10^{16} m^{-3}, electron temperature (T_e) of ~4 eV, plasma flux (Γ) of 2.0–5.0 × 10^{20} m^{-2} s^{-1}, and fluence (Φ) of 0.4–1.0 × 10^{22} m^{-2} (measured on-axis using an RF compensated Langmuir probe (LP) placed ~1 cm above the sample surface). A negative bias was applied to the tantalum (Ta) sample holder during each irradiation to achieve different impact energies (E_i, defined as the difference between the bias and the plasma potential) between 20 eV and 100 eV. A type K thermocouple placed against the bottom of the sample was used to estimate the surface temperature (thermal insulation of the SiC/graphite interface was assumed to be negligible). Exposures were performed at sample temperatures (T_s) of 500 ± 50 K and 950 ± 50 K. Lower temperature exposures were conducted using active (manual) air cooling to achieve the desired sample temperature. Higher temperature exposures were conducted by heating a HeatWave Labs, Inc. barium tungsten dispenser cathode placed behind the sample (conductive heat transfer). Additional exposures were conducted in the PISCES-A reflex arc plasma source at a flux ~10^{22} m^{-2} s^{-1} and a fluence of ~10^{25} m^{-2}. Higher fluences could be achieved on this device than on PISCES-E, yielding statistically significant levels of erosion that could not be achieved using PISCES-E on a reasonable time scale.

Before and after exposure, the mass of each sample was measured using an Ohaus Explorer Semi-Micro Balance with a resolution of 0.01 mg. An absolutely calibrated Avantes AvaSpec-ULS2048 four channel, fiber optic survey spectrometer was used during each irradiation to measure radiative emission between 350 nm and 755 nm. Photon intensities presented throughout the paper were first background

subtracted and then corrected via an absolute calibration. The instrumental width of the spectrometer was ~0.3 nm full width at half maximum (FWHM) and the integration time was adjusted between 100 ms and 1000 ms. Center wavelength (CWL) values of D-Balmer lines were used for wavelength calibrations. S/XB (ionizations per photon) values from the Atomic Data and Analysis Structure (ADAS) database [30] and D/XB (dissociations per photon) values from [31,32] were used in conjunction with the measured spectral intensities to estimate material erosion. D retention was measured post-mortem via thermal desorption spectroscopy (TDS) using a D_2 gas leak to calibrate the signal. During TDS, samples were heated in a quartz tube using radiant heaters to a maximum temperature of 1300 K with a linear ramp rate of 0.5 K/s. The surface composition was also measured before and after plasma exposure via Auger Electron Spectroscopy (AES); Ar^+ ion sputtering was used during AES measurements to remove surface oxides and obtain depth profiles.

3. Material erosion and surface enrichment

The results presented below provided insight into the intensity and identity of eroded particles during plasma exposure. A combination of microbalance data, emission spectroscopy, and Auger electron spectroscopy was used to determine if SiC has favorable erosion properties in a fusion environment.

3.1. Mass loss

Microbalance data was collected from select exposures to compare total erosion yields between different samples and provide a reference point for spectroscopic quantification (presented in Section 3.2). Erosion data collected from an exposure in PISCES-A at $E_i = 100$ eV, $T_s = 500$ K, and $\Phi \sim 10^{25}$ m^{-2} is listed in Table 1. The mass loss from the SiC sample was ~1/3 of that from the graphite sample. However, assuming that half of the particles eroded from SiC are Si atoms, the effective erosion yield (atoms removed per incident ion) was closer to 1/4 of that from graphite. The validity of this assumption will be addressed in Section 3.4. The erosion depth, Δl, of SiC was about 1/5 of that of graphite. The amount of W erosion was very low, and was likely due to the removal of surface impurities, since the D → W sputtering threshold is ~250 eV [33]. Low levels of SiC erosion, relative to graphite, justified more detailed analysis during plasma exposure.

3.2. Emission spectroscopy

In situ diagnosis of eroded material was performed using optical emission spectroscopy to resolve the contribution of different plasma-material interactions to the overall erosion intensity. Most of the analysis focuses on using the CD molecular emission band to quantify the chemical sputtering of C atoms from SiC and graphite surfaces during plasma exposure.

The total erosion of C atoms can be characterized via the C I neutral emission band (711 nm). However, the C I bands in the visible spectrum proved too weak to measure with the survey spectroscopy system. Ionic emission lines of carbon (e.g., C II) were also not observed in any exposure, which was likely due to the low T_e (~4 eV) in the PISCES-E plasma column that resulted in low levels of C ionization. C II emission has not been observed in other linear device experiments at similar values of T_e [31]. In confinement devices, deep plasma detachment (yielding a low value of T_e) has also resulted in sharp decreases in C II intensity [34].

The chemical erosion of C atoms was characterized separately by measuring the CD spectral emission signal. The chemical erosion flux of C atoms (Γ_C^{chem}) can be approximated by quantifying spectral emission lines attributed to the interaction of emitted hydrocarbons with the plasma via the D/XB method [35]. The D/XB coefficient is a ratio of the number of dissociation events to the number of photons emitted from the surface [36]. Using specific spectral emission lines (CD Gerö band and C_2 Swan band) in the measured wavelength range (355–750 nm) yields the following equations [34]:

$$\Gamma_C^{chem} = \widetilde{\Gamma}_C^{CD_x}\left[1 + \frac{\phi^{C_2}_{d^3\Pi\rightarrow a^3\Pi}}{\phi^{CD}_{A^2\Delta\rightarrow X^2\Pi}}\beta\right] \quad (1)$$

$$\widetilde{\Gamma}_C^{CD_x} = 4\pi\phi^{CD}_{A^2\Delta\rightarrow X^2\Pi}\left[\frac{D}{XB}\right]^{CD_x\rightarrow CD}_{A^2\Delta\rightarrow X^2\Pi} \quad (2)$$

where $\widetilde{\Gamma}_C^{CD_x}$ represents the apparent CD particle flux, $\phi^{C_2}_{d^3\Pi\rightarrow a^3\Pi}$ represents the photon flux from the C_2 Swan band, $\phi^{CD}_{A^2\Delta\rightarrow X^2\Pi}$ represents the photon flux from the CD band, $\left[\frac{D}{XB}\right]^{CD_x\rightarrow CD}_{A^2\Delta\rightarrow X^2\Pi}$ represents the D/XB coefficient for the CD band, and β represents the branching ratio (contribution of heavier hydrocarbons to particle flux). The C_2 Swan band, with a band head at 516.6 nm, was not detected during any exposure [35]. The relatively "cold" plasma conditions in PISCES-E were likely insufficient to drive dissociation of eroded C_2D_y; previous HYDKIN calculations found that the $\left[\frac{D}{XB}\right]^{C_2H_4\rightarrow C_2}_{d-a}$ was 25× higher in detached plasma conditions (lower T_e) than in attached plasma conditions (higher T_e) [37]. For a given erosion rate, higher D/XB coefficients correlate with weaker spectral signals. Therefore, the C_2 Swan band emission was assumed to be negligible relative to the CD Gerö band emission, simplifying equation (1) to the following:

$$\Gamma_C^{chem} = \widetilde{\Gamma}_C^{CD_x} = 4\pi\phi^{CD}_{A^2\Delta\rightarrow X^2\Pi}\left[\frac{D}{XB}\right]^{CD_x\rightarrow CD}_{A^2\Delta\rightarrow X^2\Pi} \quad (3)$$

The CD band consists of the (0,0), (1,1), and (2,2) vibrational transitions. Due to the overlap of the (0,0) and (1,1) transitions [35], only

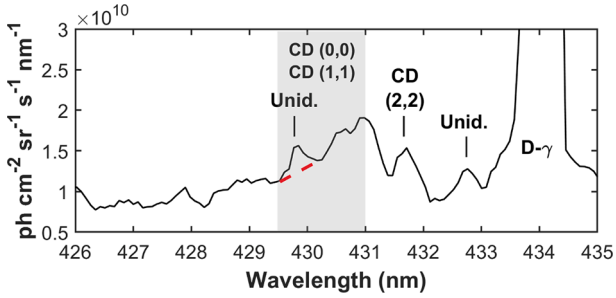

Fig. 2. Average intensity vs. wavelength during plasma exposure of SiC sample at $E_i = 50$ eV, $T_s = 500$ K, and $\Gamma_{D^+} \sim 2.0 \times 10^{20}\ m^{-2}\ s^{-1}$; centered around the CD Gerö band. The dashed red line shows removal of contaminant line (429.8 nm). The gray band denotes the integrated region. (For interpretation of the references to colour in this figure legend, the reader is referred to the web version of this article.)

Table 1
Mass loss, erosion depth, and effective erosion yield determined from microbalance data of samples exposed in PISCES-A.

Sample	T_s (K)	E_i (eV)	Φ (10^{24} m^{-2})	Δm (mg)	Δl (μm)	Y_{total} (atoms/ion)
SiC	500	100	9.8	0.13 ± 0.06	1.4 ± 0.6	0.017 ± 0.003
graphite	500	100	9.8	0.35 ± 0.06	7.0 ± 1.2	0.064 ± 0.010
W	500	100	9.8	0.03 ± 0.02	0.06 ± 0.03	0.0004 ± 0.0002

two signals were observed during the irradiation of SiC at an impact energy of 50 eV and a sample temperature of 500 K (Fig. 2). The (0,0) and (1,1) transitions produce a monotonically increasing peak with a band head at 431.0 nm, while the (2,2) transition produces a more symmetric peak with a maximum at 431.7 nm. A contaminant line was also observed with a maximum at 429.8 nm, which may have been due to Ta I (430.3 nm) emission originating from the Ta sample cap.

The total CD photon flux was calculated by subtracting the contaminant line (as indicated by the dashed red line in Fig. 2), integrating 1.5 nm in the blue direction from the CD band head, and multiplying by a correction factor to account for the rest of the spectral signal, as performed in [34]. A D/XB coefficient for the CD band has not been previously calculated at the low n_e present in PISCES-E. Therefore, an extrapolation was done based on previous D/XB measurements made in PISCES-B. Fig. 3 shows D/XB values measured from different confinement and linear devices at $T_e < 20$ eV [31,32,38–42]. Linear device measurements were chosen for extrapolation instead of those made in a confinement device to more closely mirror the plasma conditions in PISCES-E. Applying a power-law curve fit to the PISCES-B data yielded the following equation:

$$\left[\frac{D}{XB}\right]^{CD_x \rightarrow CD}_{A^2\Delta \rightarrow X^2\Pi} = (1.19 \times 10^{18}) n_e^{-0.894} \quad (4)$$

with a coefficient of determination (R^2) = 0.74. At $n_e = 3 \times 10^{16} m^{-3}$, $D/XB = 2215$. The authors acknowledge that different curve fits and different data sets will yield drastically different D/XB values. The quantitative analysis is intended to be comparative between SiC and graphite samples. Future measurements of D/XB at the low n_e ($<10^{17}$ m^{-3}) measured in the PISCES-E plasma column will provide more accurate estimates of the true D/XB value. For now, the approximate value is sufficient for initial estimates of SiC and graphite chemical sputtering.

The sputtering yield of chemically-eroded carbon particles was estimated as $Y_C^{chem} = \Gamma_C^{chem}/\Gamma_{D^+}$, where Γ_{D^+} represents the incident deuterium ion flux. Fig. 4 shows calculated Y_C^{chem} values for SiC and graphite samples at different values of E_i. Y_C^{chem} values calculated from exposures on pure Si samples were used for background subtraction to account for errant sources of carbon. Error bars represent a 3% relative error in calibration, a 0.05 mm error in the sample diameter, the root mean square error from fitting the contaminant line, the standard deviation in the flux, and the standard error of the mean sputtering yield. Y_C^{chem} values calculated using analytic equations defined in [43] for a carbon surface are also plotted as a point of reference. Neither the experimental data nor the analytic curve exhibit significant variation in Y_C^{chem} with E_i. In general, the calculated carbon chemical sputtering yield was found to be lower from SiC than from graphite. On average, the sputtering yield estimated from SiC was ~4× lower than that from graphite. The analytic curve from [43] fell within or close to the error bars of many of the estimated carbon chemical sputtering yield values from graphite, indicating that the D/XB value may be a close approximation to the true value. The accuracy of the high Y_C^{chem} values estimated for graphite at 5 eV and 10 eV is difficult to assess because it is outside of the domain of the analytic curve.

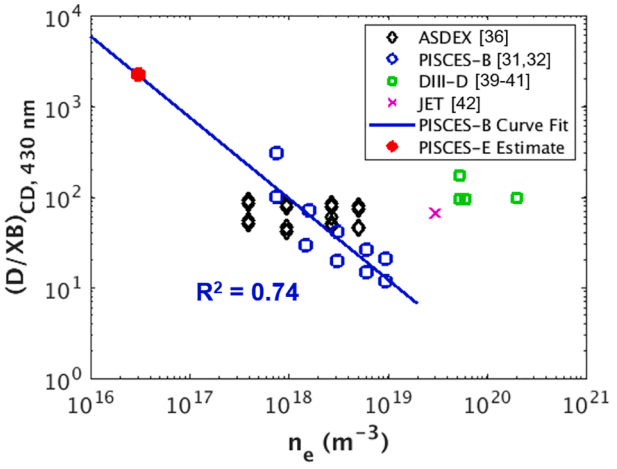

Fig. 3. D/XB values for the CD molecular emission band at 430 nm measured from different linear and confinement devices at $T_e < 20$ eV. A curve fit was applied to the PISCES-B data (blue, solid line) to estimate a D/XB value (red dot) for the n_e measured in the PISCES-E plasma column. (For interpretation of the references to colour in this figure legend, the reader is referred to the web version of this article.)

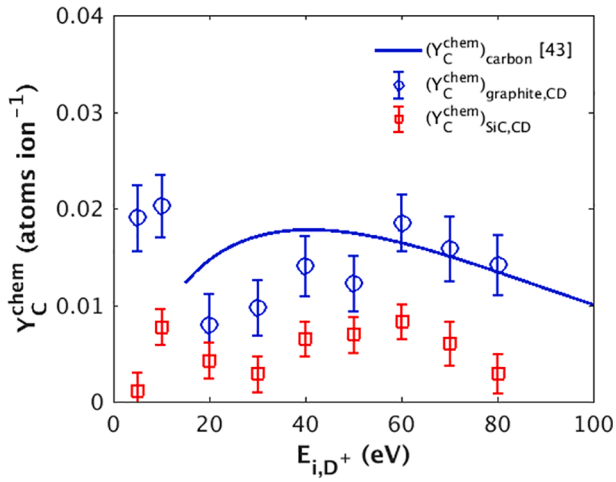

Fig. 4. Sputtering yield of carbon from silicon carbide and graphite samples vs. deuterium impact energy. Experimental sputtering yield values were calculated from emission spectroscopy data using the extrapolated D/XB coefficient in Fig. 3. The analytic equation used in [43] to calculate the chemical carbon sputtering yield from carbon is plotted for reference.

The total erosion of Si atoms can be quantified via the Si I or Si II emission band. However, no Si I or Si II lines in the measured wavelength spectrum were observed throughout PISCES-E exposures. The average emission intensities in the Si I and Si II peak regions were approximately equal to the noise level of the spectrometer. Si atoms may have been eroded during plasma exposure, but did not ionize and undergo the 4s-4p electronic transition. The lack of both the C II and Si II ionic emission signals were attributed to the very low n_e and low T_e in the PISCES-E plasma column; this is discussed further below.

The chemical erosion of Si atoms has been previously characterized via the SiD molecular emission band. Deuterated silane molecules (SiD_4) undergo a complex, plasma-induced dissociation process once they leave the sample surface [44]. The $A^2\Delta$-$X^2\Pi$ electronic transition of SiH/SiD produces a wide molecular band that can be detected between 410 nm and 425 nm. The most distinct feature of the molecular emission band, as seen in [45], is the 0–0 vibrational transition with a sharp peak ~414 nm. However, similar to the Si I and Si II peaks, the average emission intensity between 410 nm and 425 nm was approximately equal to the noise level of the spectrometer, suggesting that chemical erosion of silicon was either negligible or below the sensitivity of the spectrometer at these plasma conditions.

3.3. Surface composition

An alternative *ex situ* method for indirectly diagnosing erosion of a binary compound is the use of Auger electron spectroscopy (AES). The surface composition of SiC samples was measured before and after plasma exposure to determine if one species (Si or C) was being preferentially eroded by incident D^+ ions. Based on the escape depth of Auger electrons emitted from Si and C atoms, the maximum interaction depth is a few nm into the sample [14].

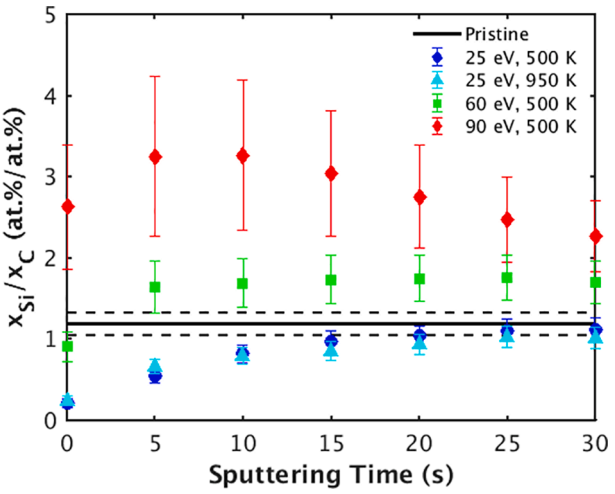

Fig. 5. Ratio of Si surface composition to C surface composition (atomic basis) vs. Ar^+ sputtering time for SiC samples exposed at $\Phi \sim (9.0 \pm 1.5) \times 10^{23}$ m^{-2} and a range of different D^+ impact energies and sample temperatures.

Depth profiling was performed via Ar^+ ion sputtering to determine how the composition evolved in the near-surface region. Fig. 5 shows the ratio of the Si composition to the C composition measured from SiC samples as a function of Ar^+ sputtering time after plasma exposures at different E_i and T_s values. Error bars reflect the variability in composition measurements at different points along the sample surface. The composition ratio of a pristine sample is indicated by a solid black line (error is denoted by dashed lines). Only the sample exposed at 90 eV exhibited Si enrichment right at the surface (0 s sputtering). However, 5 s of sputtering produced a significant increase in the Si/C composition ratio for the 60 eV and 90 eV exposures, indicating that the sample surface was covered in a small layer of C due to removal from a vacuum environment. Si enrichment was higher due to exposure at 90 eV than at 60 eV. Peak levels of Si enrichment were measured from the sample exposed at 90 eV after 5–10 s of Ar^+ sputtering, while the degree of Si enrichment remained relatively constant from the sample exposed at 60 eV as a function of sputtering time (or depth). Exposures performed at 25 eV appeared to be C rich, even after 20 s of Ar^+ sputtering. The mechanism driving C enrichment at low E_i is unclear, since the presence and intensity of Si-based erosion cannot be quantified from the measurements in this paper. The degree of C enrichment between the sample exposed at 500 K and the sample exposed at 950 K was not significantly different, regardless of depth. After 30 s of Ar^+ sputtering, the samples exposed at 90 eV and 60 eV remained Si rich, while the samples exposed at 25 eV had a composition very similar to that measured from a pristine sample.

3.4. Discussion

At low impact energies, SiC may be more resistant to chemical erosion than graphite. Mass loss data presented in Table 1 showed that at $E_i = 100$ eV, the Y_{total} of SiC is ~3× lower than that of graphite. TRIM.SP simulations conducted at these conditions found that Y_C^{phys} values for the two atomic species should be within 14% of each other. The discrepancy between Y_{total} values and Y_C^{phys} values may be due to higher Y_C^{chem} values from graphite than from SiC. Y_C^{chem} values calculated via the D/XB method were 4× lower, on average, from SiC than from graphite. However, depending on the impact energy, this difference varied between a factor of 2 and a factor of 16. As shown by the analytic curve [43] in Fig. 4, the carbon chemical sputtering yield is not expected to vary to that degree. A higher signal-to-noise ratio, higher particle flux, and higher exposure time may reduce fluctuation in the CD spectroscopy measurements. CH spectroscopy measurements conducted in [13] do support the general observation that carbon chemical erosion from SiC is lower than that from graphite; plasma exposures in Pilot-PSI measured a 10× lower photon flux from SiC than from graphite. In addition, while the relative difference in Y_C^{chem} between graphite and SiC varied significantly depending on impact energy, the overall trend for each sample was fairly flat (especially when considering error bars). D^+ ion irradiations of graphite samples at 500 K also found that increasing the impact energy from 10 eV to 100 eV did not substantially change the carbon chemical erosion yield [46]. While additional spectroscopic measurements of CD emission may help further clarify the precise differences in erosion between SiC and graphite, the data shown in Fig. 4 suggests that, in general, SiC exhibits less chemical sputtering of carbon than graphite and that changing the impact energy between 10 eV and 100 eV does not substantively affect this observation.

Chemical erosion of Si was not detected via emission spectroscopy on SiC or Si, suggesting that silane molecules either dissociated too quickly for the spectrometer to detect them or did not dissociate at all. The complete absence of SiD spectral emission from either SiC or Si in PISCES-E makes it difficult to draw conclusions on the presence or absence of Si chemical erosion during plasma exposure. Si surface enrichment was only observed at 60 eV and 90 eV, and not at 25 eV (Fig. 5). If the physical sputtering thresholds of Si and C on SiC are 25 eV and 20 eV (obtained from TRIM.SP [47]), respectively, then the onset of Si surface enrichment may be due to preferential carbon erosion by physical sputtering, as opposed to chemical erosion. TRIM.SP simulations conducted for D on SiC found that Y_C^{phys} was 4.5× higher than Y_{Si}^{phys} at 50 eV and 1.8× higher at 90 eV. Therefore, Si enrichment at impact energies above $E_{threshold}$ can be attributed to preferential physical sputtering of carbon. At 20 eV, Y_C^{chem} was estimated to be ~0.004 but Si enrichment was not observed, implying that Y_{Si}^{chem} was likely not zero. Significant Si II emission has been measured at low T_e from SiC samples in DIII-D [27]. Temporally-resolved, *in situ* surface composition measurements may help track the potential growth and/or erosion of enriched Si layers on the SiC surface. Silane injection studies in [48] suggested that Si II emission can be used as an indirect measurement of silane content. Future work should attempt to directly measure the presence of silane molecules at low E_i.

As discussed above, the lack of C and Si ionic emission during plasma exposure was likely due to the plasma conditions in PISCES-E and did not necessarily imply that material erosion was negligible. Measurable levels of SiC mass loss, CD emission, and changes in the surface composition suggest that material was eroded from the SiC surface during plasma exposure. Observation of ionic spectroscopic emission requires an eroded Si or C atom to erode, ionize, and then subsequently undergo an electronic transition. Assuming a uniform $n_e \sim 3 \times 10^{16}$ m^{-3} and $T_e \sim 4$ eV, the ionization mean free path of C^0 in the PISCES-E plasma column is ~3 m. Since the FWHM of the plasma beam is ~0.03 m, the ionization of eroded Si and C atoms is very unlikely within the plasma. Increasing n_e by factor of 100 to match that measured in the edge of confinement devices (n_e near DiMES ~ 10^{18} – 10^{20} m^{-3} [26]) yields a mean free path of ~0.04 m, which explains the significant C II emission and Si II emission observed from DiMES SiC samples in [26,27]. Future work should either 1) pursue material testing in linear devices that can produce denser plasmas or 2) characterize neutral emission lines to track total erosion. The C I multiplet at 910 nm and the Si I signal at 288 nm are the best candidates for erosion quantification using neutrals [48,49], but both lie outside of the visible range. Ultraviolet (UV) and near-infrared (NIR) spectrometers are therefore required to measure these signals. Future work will explore different options to better characterize total Si and C erosion using emission spectroscopy.

Depth-resolved composition measurements of exposed SiC samples revealed that Si enrichment may be primarily driven by C physical sputtering. The use of Ar^+ sputtering helped remove buildup of carbon

and other surface impurities to reveal changes to the near-surface region due to interactions with incident D^+ ions. Both the 60 eV and 90 eV exposures caused Si enrichment, while the 25 eV exposures at 500 K and 950 K caused C enrichment. However, the Si/C composition ratio measured from the sample exposed at 90 eV was up to 2× higher than the Si/C composition ratio measured from the sample exposed at 60 eV. The significant difference in Si enrichment between samples cannot be explained by carbon chemical sputtering, since Y_C^{chem} did not vary with impact energy, as shown in Fig. 4. The difference is therefore likely due to large changes in Y_C^{phys} below 100 eV; Y_C^{phys} is ~3× higher at 90 eV than at 60 eV as calculated by SDTRIM.SP [27]. In contrast, $Y_{Si}^{phys} \sim 0$ below 100 eV [27]. While the comparatively low Si/C composition ratio at the surface is thought to be due to impurity buildup from the ambient environment, the sustained enrichment in C with increasing depth for samples exposed at 25 eV cannot be explained by existing measurements of sputtering from SiC. The presence of Si enrichment at higher impact energies is thought to be due to the onset of C physical sputtering, but below 30 eV, $Y_C^{phys} \sim 0$ [27]. In the absence of C physical sputtering ($Y_C^{phys} \sim 10^{-3}$–10^{-2}), C chemical sputtering ($Y_C^{chem} \sim 10^{-3}$–10^{-2}) would still produce a Si-enriched surface with significant overall erosion to be detected, but that was not observed. Results presented in [12] also noted a lack of Si enrichment after 20 eV D plasma irradiation of a SiC sample, intimating that Si is being eroded from the surface via chemical, non-collisional processes that were not detected. The ambiguity surrounding the presence of Si chemical erosion necessitates further research using innovative, high-resolution erosion measurement techniques during long-duration plasma exposures (better statistics).

4. Retention of implanted deuterium

For use in a fusion reactor, high-performance silicon carbide PFCs must exhibit low hydrogenic retention to stay below administrative limits on tritium build-up and facilitate a sustainable fuel cycle. While overall D retention in SiC may be dominated by co-deposition if deployed as a PFC in a toroidal device, experiments performed in linear devices suggest that SiC may exhibit a lower co-deposition rate than that of graphite [50]. Co-deposition will be negligible in W at low plasma fluences, due to its low physical sputtering yield [51] but some recent work suggests that co-deposition may dominate the total tritium retention in W at higher fluences expected in a power-producing reactor [52]. Therefore, comparing retention due to ion implantation between different PFC candidate materials provides a useful lower bound for evaluation. Currently, the magnitude of retention and behavior of trapped hydrogenic species caused by low-energy ion implantation has not been extensively studied in SiC. In this work, post-mortem thermal desorption spectroscopy (TDS) was used to quantify the retention and characterize the trapping behavior of implanted deuterium in SiC.

4.1. Thermal desorption spectra

The shape and temperature of desorption peaks partially reveal how deuterium is trapped in materials during plasma exposure. In this paper, a "trap" specifically refers to a defect in the SiC lattice where D atoms may reside. TDS spectra of the normalized D_2 desorption flux vs. temperature measured from plasma exposures on SiC at different E_i (±5 eV) are plotted in Fig. 6. All SiC samples exhibited one major desorption peak at a temperature between 900 K and 1020 K. Increasing E_i shifted the desorption peak to lower temperatures. The spectrum measured from the 100 ± 5 eV D → SiC exposure exhibited a major peak around 910 K and a second, minor peak around 1000 K. The spectrum measured from the 25 ± 5 eV exposure exhibited the widest peak shown, which may have been due to its comparably low signal-to-noise ratio (lowest D_2 desorption intensity). The results shown represent the first desorption spectra published at a range of impact energies for deuterium plasma exposures on SiC, to the best of this author's knowledge. Fig. 7 shows the difference in normalized D_2 desorption flux spectra at two

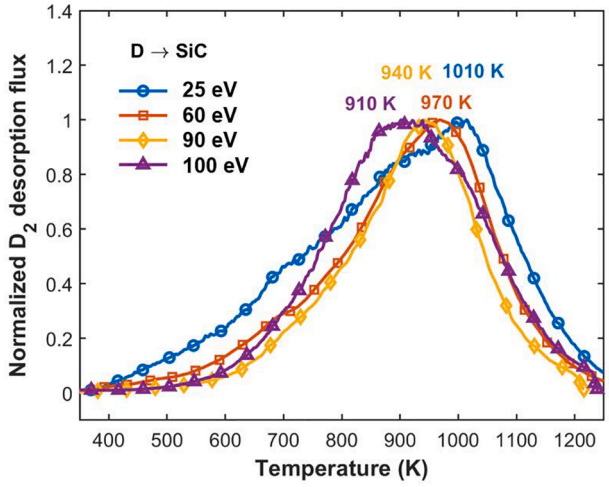

Fig. 6. Normalized D_2 desorption flux vs. sample temperature from SiC samples exposed at different impact energies; $T_s = 500$ K.

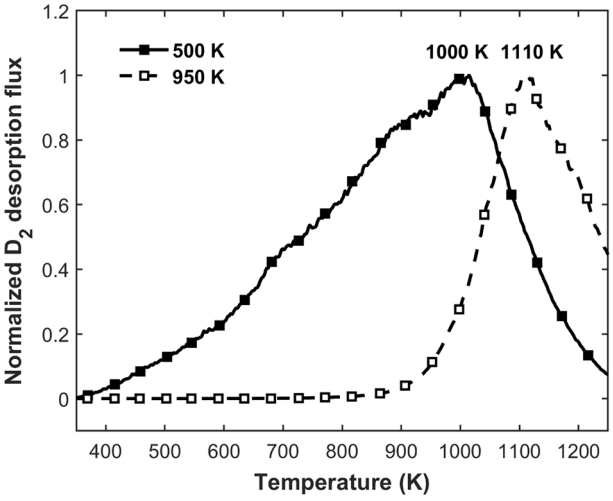

Fig. 7. Normalized D_2 desorption flux vs. sample temperature from SiC samples exposed at $T_s = 500$ K & 950 K; $E_i = 25 \pm 5$ eV.

different exposure temperatures, 500 K and 950 K, at $E_i = 25 \pm 5$ eV. The maximum desorption temperature shifted from 1000 K ($T_s = 500$ K) to 1110 K ($T_s = 950$ K). As expected, the desorption flux below ~900 K is negligible for the $T_s = 950$ K case due to thermally-induced desorption during plasma exposure.

Comparing TDS spectra between SiC, Si, and graphite samples exposed simultaneously may reveal the contributions of C traps and Si traps to SiC retention behavior. The normalized D_2 desorption flux vs. temperature spectra obtained from SiC, graphite, and Si samples exposed at $T_s = 500$ K and $E_i = 100 \pm 5$ eV are plotted together in Fig. 8. As mentioned in the previous paragraph, the SiC desorption spectrum exhibits a major peak ~910 K and a minor peak ~1000 K. The graphite spectrum has one broad, major peak centered around 880 K. The Si spectrum has two major peaks at 820 K and 900 K. Both the Si and graphite spectra also have a minor peak between 600 K and 700 K. Finally, the graphite spectrum exhibits a significant low-temperature tail while the Si spectrum exhibits a significant high-temperature tail. The similarity in desorption spectra between Si and graphite makes it difficult to conclude that trapping in SiC is clearly represented by a superposition of C-based trapping sites and Si-based trapping sites, as determined in [20,21,53–55]. The temperature of the major desorption peaks from SiC, graphite, and Si samples are all somewhat similar, but

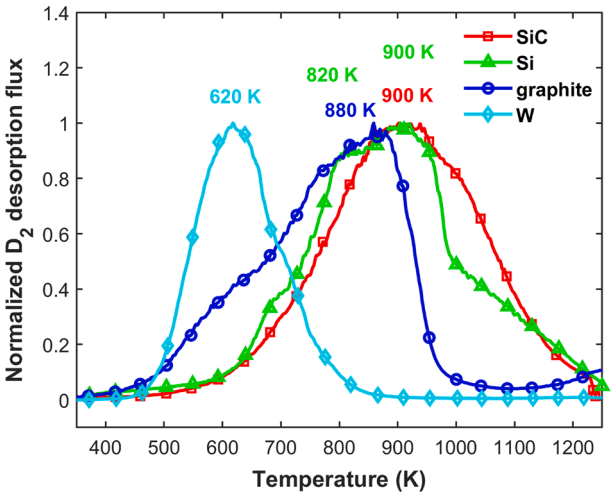

Fig. 8. Normalized D_2 desorption flux vs. sample temperature from SiC, W, Si, and graphite samples exposed at $T_s = 500$ K, $E_i = 100 \pm 5$ eV, and $\Phi \sim 4.5 \times 10^{23}$ m^{-2}. Maximum desorption temperatures from each sample spectrum have been noted.

the minor peak at 1000 K present in the SiC spectrum cannot be found in either the graphite spectrum or the Si spectrum. The presence of this peak may be due to additional defects that are unique to a cubic SiC lattice.

The normalized D_2 desorption flux vs. temperature spectrum obtained from a W sample is plotted in Fig. 8 alongside SiC, Si, and graphite samples that were all exposed simultaneously at $E_i = 100 \pm 5$ eV and $T_s = 500$ K. The W sample exhibited a peak desorption temperature of 620 K, which is almost 300 K lower than the peak desorption temperature from the SiC sample. The overall desorption peak was also much narrower in W than in SiC, with a FWHM that was half that of SiC. Estimates of total D retention from exposures on SiC and W samples are plotted in Fig. 9 as a function of E_i and listed in Table 2 with associated exposure conditions. Error bars represent a 15% relative error in the D_2 leak calibration. The D retention was 1.6–2.6× higher in SiC than in W, depending on the impact energy. In addition, the D retention was higher at higher E_i, but quantifying the change is difficult due to the error in retention measurements. The exposure performed at 79 eV yielded significantly lower retention values than obtained from other exposures,

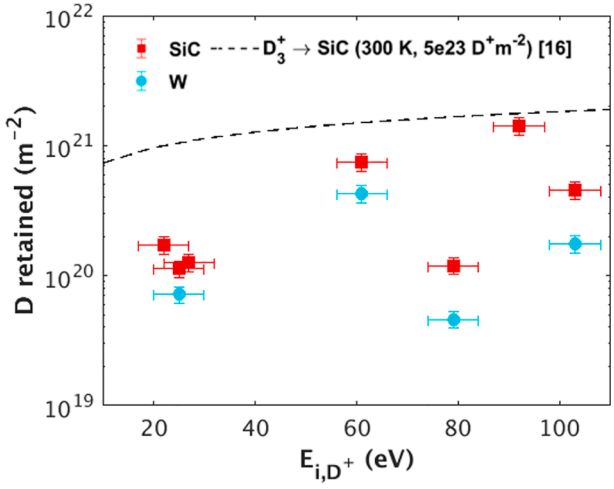

Fig. 9. Deuterium retention vs. impact energy calculated from exposures on SiC and W samples at different fluences and a constant $T_s = 500$ K. Extrapolation of the trendline fit to data taken in [16] on similar samples at higher impact energies is plotted for reference.

Table 2
Measured D retention of SiC and W samples exposed to D plasma irradiation in PISCES-E at $T_s = 500$ K and a range of impact energies (E_i) and fluences (Φ).

E_i (eV)	Φ (10^{24} m^{-2})	Retention (SiC) (10^{20} D m^{-2})	Retention (W) (10^{20} D m^{-2})
92 ± 5	1.0 ± 0.1	14 ± 1	
22 ± 5	0.75 ± 0.10	1.7 ± 0.1	
61 ± 5	0.88 ± 0.10	7.5 ± 0.4	4.3 ± 0.4
103 ± 5	0.45 ± 0.10	4.6 ± 0.1	1.8 ± 0.1
25 ± 5	0.42 ± 0.10	1.1 ± 0.1	0.71 ± 0.01
27 ± 5	0.48 ± 0.10	1.2 ± 0.1	
79 ± 5	0.54 ± 0.10	1.2 ± 0.1	0.46 ± 0.03

and is considered to be an outlier. A trendline (equation: Retention/$\Phi = (2.94 \times 10^{20}) E_i^{0.397}$) fit to retention measurements on the same SiC samples after plasma exposures performed at $T_s = 300$ K, $\Phi = 5 \times 10^{23}$ m^{-2}, and E_i between 500 eV and 3 keV in [16] was extrapolated to lower values of E_i and plotted on the same graph for reference. The trendline overestimates all retention measurements, but diverges increasingly with decreasing E_i. Significant differences in retention between studies implies that ion-induced displacement damage present at $E_i \sim 1$ keV likely contributed to different types of trapping not observed at lower impact energies [56]. While the degree of retention due to ion implantation appears to be similar between SiC and W, the onset of co-deposition in a toroidal device will preferentially increase the effective D inventory in SiC.

4.2. Discussion

The D_2 desorption spectra measured from exposures on SiC between 25 eV and 100 eV are different than those obtained in previous studies at higher impact energies. Among the few retention measurements that have been previously been done on D-exposed SiC, all of them were performed at higher impact energies. TDS spectra obtained in many different papers all show two distinct peaks for SiC – one around 800–900 K and another one around 1000–1100 K [20,21,53–55]. The lower temperature peak closely matches the TDS spectra obtained from a silicon sample and the higher temperature peak closely matches the TDS spectra obtained from a graphite sample. Changes in the shape of the SiC desorption peak with Φ or T_s are therefore attributed to changes in the relative intensities of D-Si bonds and D-C bonds. In this paper, the SiC spectrum does not exhibit two distinct peaks and the Si and graphite spectra have a different shape than the spectra previously observed at higher values of E_i. For example, the Si spectrum in [21] contains three peaks – 500 K, 620 K, 810 K. The Si spectrum shown in Fig. 8 only contains two peaks at 820 K and 900 K. The trapping of D in SiC measured from these exposures cannot confidently be described as a combination of trapping in C and trapping in Si.

The difference in retention behavior between previous studies and the results presented in this paper can likely be attributed to the large difference in the population of ion-induced traps at $E_i < 100$ eV versus $E_i > 1$ keV. In tungsten, the rate of ion-induced defect production increases with E_i [57]. In the absence of ion-induced defects, implanted D is trapped primarily at intrinsic defects in the material, such as grain boundaries, dislocations, and vacancies [57]. Extending that logic to SiC means that implanted D is trapped at fundamentally different defects in the material, depending on E_i. The trendline shown in Fig. 9 was extrapolated from retention measurements acquired between D impact energies of 500 eV and 3 keV, and appears to be overestimating total D retention at lower E_i [16]. Additional ion-induced displacement damage at higher E_i produces more defects and creates new trapping sites that are not present at low E_i. Dedicated modeling of D desorption (via reaction–diffusion codes) will be needed to more precisely define the contribution of Si atoms and C atoms to trap formation and gas migration in a SiC lattice; such efforts are outside the scope of this paper.

The total amount of D retention measured in SiC and W samples after

exposure at a surface temperature of 500 K and a fluence between 0.40 and 1.0×10^{22} m^{-2} appear to be similar in magnitude across a range of impact energies. The primary difference can be observed in the desorption spectra; most D retained in SiC is trapped at a much higher desorption temperature. As seen in Fig. 9, retention in SiC was 1.6–2.6× higher than in W over the range of impact energies investigated. The major desorption signal in SiC exhibits a higher peak desorption temperature and a larger FWHM than that for W, making efficient tritium removal more difficult with SiC PFCs. However, if future fusion devices utilize hot walls for thermodynamic efficiency, with temperatures exceeding 900 K, thermally-induced desorption during operation may make these differences in static desorption temperatures less relevant [58,59].

Comparing retention data obtained in this study with previous work reveals that current predictions of retention do not scale properly to low impact energies. Increases in retention observed in Fig. 9 for both W and SiC with increasing E_i up to 100 eV is to be expected, based on similar observations in W in [60]. Increasing the impact energy in this regime will induce additional stress on the material lattice, increasing the effective trap concentration of implanted D, as explained in [60]. However, the trendline plotted in Fig. 9 significantly overestimates the measured retention values because it was based on exposures performed at higher impact energies ($E_i \sim 1$ keV), where the addition of ion-induced defects are expected to significantly increase the effective D retention [16]. Predictions of retention behavior in SiC PFCs need to be readjusted to account for differences in displacement damage with impact energy.

A dedicated fluence parameter scan over multiple decades (at a constant flux) is needed to determine if the retention in SiC and in W increase at the same rate with time. Retention in SiC is expected to increase at a slower rate due to its lower hydrogenic diffusivity, as discussed in [2]. Quantifying deuterium retention in both SiC and W samples exposed to the same plasma conditions provided valuable comparisons between two PFC candidate materials. Finding that retention by implantation in SiC was somewhat similar to that in W justifies further testing in a confinement device where co-deposition can be quantified. Expanded testing on SiC is key to fully determining its compatibility in a high-performance fusion environment.

5. Conclusion

Emission spectroscopy and thermal desorption spectroscopy were used to characterize the erosion and retention of SiC in a deuterium plasma at divertor-relevant ion impact energies. Observation of the CD Gerö band during irradiation was linked to the chemical erosion of C atoms on the SiC surface. Quantification of the CD band via the D/XB method found that the carbon chemical sputtering yield from SiC varied between 0.0012 and 0.0083, which was 4× lower than that calculated from graphite (on average). The magnitude of carbon chemical sputtering for both samples did not significantly vary with impact energy. A more expanded CD D/XB coefficient database could improve the accuracy of the spectroscopic erosion calculations. Neither carbon nor silicon ionic emission lines were observed due to the long Si and C ionization lengths in the plasma column. Direct evidence of silicon chemical erosion via the SiD molecular emission band was not observed from SiC or Si samples, in contrast to previous studies that have observed silane emission from Si but not from SiC [11]. Measuring the surface composition of exposed SiC samples revealed that Si surface enrichment may not be tied to the absence of silicon chemical erosion, and may, instead, be linked to higher levels of physical sputtering from C than from Si for $E_i > 30$ eV. The lack of Si enrichment below the physical sputtering threshold suggests that Si atoms must have left the surface via a non-collisional erosion process at a rate similar to that of carbon chemical erosion. Future studies should investigate more sensitive methods for detecting eroded silane. Lower levels of carbon chemical erosion measured from SiC, relative to graphite, suggest that SiC may produce a lower C erosion source in a fusion device.

One major D_2 desorption peak ~1000 K was observed during post-mortem TDS analysis of the SiC samples. This peak shifted downward in temperature with increasing E_i and upward in temperature with increasing T_s. Desorption spectra of exposed Si and graphite samples exhibited similar peak desorption temperatures, but differences in the shape of the overall desorption signal suggests that trapping of D in SiC is not simply a combination of Si-D bonds and C-D bonds, as previously seen at higher E_i. Direct comparisons with exposed W samples found that while the magnitude of retention by implantation was similar between materials across a range of E_i, the peak desorption temperature was substantially higher in SiC, which may make recovery of implanted fuel more difficult. Operating a fusion device with heated walls may alleviate this concern, particularly since silicon carbide PFCs have higher operating temperature limits than refractory metals. Differences between the retention spectra obtained in this study at $E_i < 100$ eV and those obtained in previous studies at $E_i > 1$ keV suggest that additional trapping sites at different trapping energies are created at high impact energies through ion-induced displacement damage. Energetic charge-exchange neutrals in a confinement device may possess impact energies sufficient to induce such damage in the surrounding PFCs, contributing to higher retention [61]. While additional experiments in a confinement device are necessary to better understand the contribution of co-deposition to the overall hydrogenic inventory in SiC, these results serve as an important step in qualifying SiC as a low-to-medium-Z plasma-facing material in future fusion devices.

CRediT authorship contribution statement

G. Sinclair: Conceptualization, Methodology, Formal analysis, Investigation, Data curation, Visualization, Writing - original draft, Writing - review & editing. **T. Abrams:** Conceptualization, Methodology, Software, Formal analysis, Writing - original draft, Writing - review & editing, Supervision. **S. Bringuier:** Conceptualization, Methodology, Software, Formal analysis, Writing - original draft, Writing - review & editing. **D.M. Thomas:** Conceptualization, Methodology, Writing - original draft, Writing - review & editing, Supervision, Project administration. **L. Holland:** Conceptualization, Methodology, Writing - original draft, Supervision, Project administration, Funding acquisition. **S. Gonderman:** Conceptualization, Methodology, Resources, Writing - original draft. **J.H. Yu:** Formal analysis, Investigation, Resources, Writing - original draft, Writing - review & editing. **R.P. Doerner:** Investigation, Resources, Writing - original draft, Writing - review & editing, Supervision.

Declaration of Competing Interest

The authors declare that they have no known competing financial interests or personal relationships that could have appeared to influence the work reported in this paper.

Acknowledgments

This research was supported by General Atomics Internal Research & Development. Authors would like to thank Marlene Patino, Mike Simmonds, Tyler Lynch, Emily Mathison, Ray Tao, and Howard Grunloh for their technical assistance throughout this study. Authors would also like to thank Josh Whaley for in-kind sample contribution.

References

[1] R.A. Causey, et al., J. Am. Ceram. Soc. 61 (1978) 221–225.
[2] G.M. Wright, et al., J. Nucl. Mater. 458 (2015) 272–274.
[3] A. Hasegawa, et al., J. Nucl. Mater. 283–287 (2000) 128–137.
[4] Y. Katoh, et al., J. Nucl. Mater. 417 (2011) 400–405.
[5] A.R. Raffray, et al., Fusion Eng. Des. 80 (2006) 79–98.
[6] A.Ž. Iveković, et al., J. Eur. Ceram. Soc. 33 (2013) 1577–1589.

[7] Y. Katoh, A. Kohyama, T. Hinoki, L.L. Snead, Fusion Sci. Technol. 44 (2003) 155–162.
[8] T. Hinoki, et al., Mater. Trans. 54 (2013) 472–476.
[9] G. Newsome, et al., J. Nucl. Mater. 371 (2007) 76–89.
[10] S.J. Zinkle, N.M. Ghoniem, Fusion Eng. Des. 51–52 (2000) 55–71.
[11] M. Balden, J. Roth, J. Nucl. Mater. 279 (2000) 351–355.
[12] M. Balden, S. Picarle, J. Roth, J. Nucl. Mater. 290–293 (2001) 47–51.
[13] J. Westerhout, et al., Phys. Scr. T138 (2009), 014017.
[14] H. Plank, R. Schwörer, J. Roth, Nucl. Instruments Methods Phys. Res. Sect. B Beam Interact. with Mater. Atoms. 111 (1996) 63–69.
[15] M. Mohri, K. Watanabe, T. Yamashina, J. Nucl. Mater. 75 (1978) 7–13.
[16] M.T. Koller, et al., Nucl. Mater. Energy. 20 (2019), 100704.
[17] G. Federici, et al., Nucl. Fusion. 41 (2001) 1967–2137.
[18] C. García-Rosales, W. Eckstein, J. Roth, J. Nucl. Mater. 218 (1995) 8–17.
[19] C.H. Skinner, et al., Fusion Sci. Technol. 54 (2008) 891–945.
[20] T. Hino, M. Akiba, Fusion Eng. Des. 49–50 (2000) 97–105.
[21] Y. Oya, Y. Onishi, K. Okuno, S. Tanaka, Mater. Trans. 46 (2005) 552–556.
[22] R.A. Causey, W.R. Wampler, J.R. Retelle, J.L. Kaae, J. Nucl. Mater. 203 (1993) 196–205.
[23] R.A. Causey, W.R. Wampler, J. Nucl. Mater. 220–222 (1995) 823–826.
[24] D.M. Goebel, G. Campbell, R.W. Conn, J. Nucl. Mater. 121 (1984) 277–282.
[25] G.R. Tynan, et al., J. Vac. Sci. Technol. A Vacuum, Surfaces, Film. 15 (1997) 2885–2892.
[26] D.L. Rudakov, et al., Phys. Scr. T171 (2020), 014064.
[27] T. Abrams, et al., in review, Nucl. Fusion (2021).
[28] K.J. Taylor, S. Yun, G.R. Tynan, J. Vac. Sci. Technol. A Vacuum, Surfaces, Film. 22 (2004) 2131.
[29] H.E. Khalifa, C.P. Deck, K.C. Chen, C.A. Back, Fusion Sci. Technol. 61 (2012) 375–380.
[30] H.P. Summers, Atomic Data and Analysis Structure, version 2.6, 2004. www.adas.ac.uk.
[31] D. Whyte, G. Tynan, R. Doerner, J. Brooks, Nucl. Fusion. 41 (2001) 47–62.
[32] R.P. Doerner, et al., J. Nucl. Mater. 290–293 (2001) 166–172.
[33] W. Eckstein, Calculated sputtering, reflection, and range values, IPP-9/132 (2002).
[34] S. Brezinsek, et al., J. Nucl. Mater. 363–365 (2007) 1119–1128.
[35] S. Brezinsek, et al., Phys. Scr. T111 (2004) 42.
[36] S. Brezinsek, et al., J. Nucl. Mater. 313–316 (2003) 967–971.
[37] S. Brezinsek, et al., Phys. Scr. T 128 (2007) 40–44.
[38] J. Roth, Synopsis of erosion and redeposition, in, Phys. Scr. T, IOP Publishing (2001) 65–69.
[39] A.G. McLean, Quantification of chemical erosion in the divertor of the DIII-D tokamak, PhD thesis, University of Toronto, 2009.
[40] A.G. McLean, et al., J. Nucl. Mater. 363–365 (2007) 86–90.
[41] A.G. McLean, et al., J. Nucl. Mater. 390–391 (2009) 160–163.
[42] R.D. Monk, et al., Phys. Scr. T81 (1999) 54.
[43] J. Roth, J. Nucl. Mater. 266–269 (1999) 51–57.
[44] U. Fantz, Plasma Phys. Control. Fusion. 40 (1998) 1035–1056.
[45] J. Perrin, E. Delafosse, J. Phys. D. Appl. Phys. 13 (1980) 759–765.
[46] B. Mech, A. Haasz, J. Davis, J. Nucl. Mater. 255 (1998) 153–164.
[47] J.P. Biersack, W. Eckstein, Appl. Phys. A Solids Surfaces. 34 (1984) 73–94.
[48] A. Huber, et al., Plasma Phys. Control. Fusion. 45 (2003) 89–103.
[49] R.C. Isler, et al., J. Nucl. Mater. 313–316 (2003) 873–877.
[50] R.A. Causey, J. Nucl. Mater. 313–316 (2003) 450–454.
[51] G. Federici, H. Wuerz, G. Janeschitz, R. Tivey, Fusion Eng. Des. 61–62 (2002) 81–94.
[52] R.P. Doerner, G.R. Tynan, K. Schmid, Nucl. Mater. Energy. 18 (2019) 56–61.
[53] Y. Oya, et al., J. Nucl. Mater. 337–339 (2005) 595–599.
[54] Q. Li, et al., Fusion Eng. Des. 86 (2011) 1689–1692.
[55] Y. Nobuta, T. Hino, Y. Yamauchi, T. Nozawa, J. Vac. Soc. Japan. 58 (2015) 173–176.
[56] J.F. Ziegler, M.D. Ziegler, J.P. Biersack, Nucl. Instruments Methods Phys. Res. Sect. B Beam Interact. Mater. Atoms. 268 (2010) 1818–1823.
[57] O.V. Ogorodnikova, J. Roth, M. Mayer, J. Appl. Phys. 103 (2008), 034902.
[58] Y. Wu, P. Krstic, F.Y. Zhou, F. Meyer, J. Nucl. Mater. 467 (2015) 480–487.
[59] G.M. Wright, et al., Nucl. Fusion. 50 (2010), 075006.
[60] J.P. Roszell, A.A. Haasz, J.W. Davis, J. Nucl. Mater. 415 (2011) S641–S644.
[61] M. Oya, et al., J. Nucl. Mater. 463 (2015) 1037–1040.